

A Stabilized Circuit-Consistent Foil Conductor Model

Elias Paakkunainen^{a,b,*}, Jonas Bundschuh^a, Idoia Cortes Garcia^c,
Herbert De Gersem^a, and Sebastian Schöps^a

^aInstitute for Accelerator Science and Electromagnetic Fields,
Technical University of Darmstadt, Darmstadt, Germany

^bElectrical Engineering Unit,
Tampere University, Tampere, Finland

^cDepartment of Mechanical Engineering - Dynamics and Control,
Eindhoven University of Technology, Eindhoven, Netherlands

Abstract

The magnetoquasistatic simulation of large power converters, in particular transformers, requires efficient models for their foils windings by means of homogenization techniques. In this article, the classical foil conductor model is derived and an inconsistency in terms of circuit theory is observed, which may lead to time-stepping instability. This can be related to the differential-algebraic nature of the resulting system of equations. It is shown how the foil conductor model can be adapted to mitigate this problem by a modified definition of the turn-by-turn conductance matrix. Numerical results are presented to demonstrate the instability and to verify the effectiveness of the new adapted foil conductor model.

Keywords: Foil conductor model; foil winding; differential algebraic equation; differential index; finite element method.

1 Introduction

Low-frequency electromagnetic field models are typically connected to a circuit model consisting of lumped elements to excite them [23]. This is done by means of conductor models that distribute circuit voltages and currents as electric fields and currents over the spatially resolved computational domain back and forth. The well-known terms *solid* and *stranded conductor* model have been coined in

*Corresponding author: elias.paakkunainen@tu-darmstadt.de

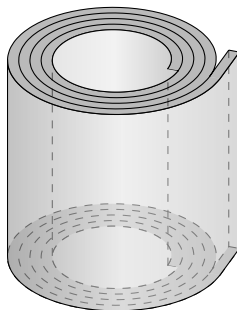


Figure 1: Illustration of the geometry of a foil winding.

Ref. [5] and refined over the years, see e.g. Refs. [13] and [28] and the references therein.

However, in some situations, e.g., transformers and inductors with foil windings, the conventional conductor models become cumbersome, e.g. since thin sheets must be resolved on the computational domain. Here, foil conductor models [11, 14, 29] have been proposed. Figure 1 illustrates the foil winding geometry.

Sometimes field equations and conductor models are embedded into circuit simulations, for example if a power converter controller is simulated along with the device of interest [21]. The numerical treatment of such coupled problems has been investigated in Refs. [6, 12, 15, 20, 25]. Two types of approaches can be distinguished: monolithic methods, where all equations are solved together in one large system, and co-simulation approaches, where the equations are solved separately with limited (possibly iterative) exchange of information. The numerical behavior of the resulting field/circuit coupled system has been analysed in Refs. [3, 4, 9, 24]. In conclusion: low-frequency magnetoquasistatic field models based on solid and stranded conductors shall be driven by voltages rather than currents to avoid numerical difficulties. This is consistent with their lumped equivalent model like (nonlinear) inductors, and it is independent of their potential formulation, i.e., $\vec{A} - \phi$ or $\vec{T} - \Omega$.

This paper extends the analysis of field/circuit coupled systems to the case of foil conductor models. We observe an issue with the conventional finite element (FE) approximation of the foil winding turn-by-turn conductance matrix and propose a new variant that restores the consistency with the inductance-like behavior of solid and stranded conductors. The structure is as follows: Section 2 introduces the foil conductor model and describes its proposed modification. Section 3 examines how the model behaves as a part of an external circuit. In Section 4, numerical results are presented to verify the findings of the previous sections.

2 Foil Conductor Model

Foil conductor models have been originally proposed in Refs. [11] and [14]. However, the following derivation follows mainly Ref. [29]. It starts with the magnetoquasistatic approximation of Maxwell's equations on a domain Ω , using the $\vec{A} - \phi$ -formulation with the magnetic vector potential \vec{A} and the electric scalar potential ϕ . Consequently, the electric field can be written as

$$\vec{E} = -\partial_t \vec{A} - \text{grad } \phi. \quad (1)$$

We choose the scalar potential such that

$$-\text{grad } \phi = \Phi \vec{\zeta} =: \vec{E}_s, \quad (2)$$

with the voltage function Φ and a distribution function $\vec{\zeta}$ defined in the foil winding domain $\Omega_{\text{fw}} := \text{supp}(\vec{\zeta})$, where $\vec{\zeta}$ corresponds to the winding function for solid conductors from Ref. [26]. We assume that its direction is perpendicular to a constant rectangular cross-section

$$S = \left[-\frac{\ell_\alpha}{2}, \frac{\ell_\alpha}{2} \right] \times \left[-\frac{\ell_\beta}{2}, \frac{\ell_\beta}{2} \right],$$

see Fig. 2a. To further simplify the notation, we introduce a local coordinate system $\alpha \in L_\alpha$, $\beta \in L_\beta$, $\gamma \in L_\gamma$ in the foil winding domain Ω_{fw} and use the (invertible) mapping $\mathbf{f} : (\alpha, \beta, \gamma) \mapsto (x, y, z)$ to transform local to global coordinates. We assume \mathbf{f} to be linear in both α and β and to map the rectangle S to a rectangle in Ω . Note that not all of these assumptions are mathematically necessary but they cover all practical relevant cases. Finally, in the third dimension, the distribution function fulfills the property

$$\int_{\mathbf{f}(\alpha, \beta, L_\gamma)} \vec{\zeta} \cdot d\vec{s} = 1, \quad \forall \alpha \in L_\alpha, \forall \beta \in L_\beta. \quad (3)$$

Let us denote the number of turns with N . Then the domain of the k -th turn is described by $\Omega_k \subset \Omega_{\text{fw}}$ such that $\Omega_{\text{fw}} = \cup_{k=1}^N \Omega_k$. On each turn we define a restricted distribution function as

$$\vec{\zeta}_k = \begin{cases} \vec{\zeta} & \text{in } \Omega_k, \\ 0 & \text{else.} \end{cases} \quad (4)$$

Figure 2b shows the cross-section of a single foil. It consists of a conducting material of width b_c and an insulation material of width b_i . The total width of one foil is b . The fill factor is defined $\lambda := \frac{b_c}{b}$. We assume, due to insulation, that the electric field perpendicular to the foils, i.e., in α -direction of the local coordinate system, does not generate a current density.

To ensure that the total current flowing through every foil is equal to a lumped current i , it must hold

$$i = \int_{\Omega} \vec{J} \cdot \vec{\zeta}_k \, dV \quad (5)$$

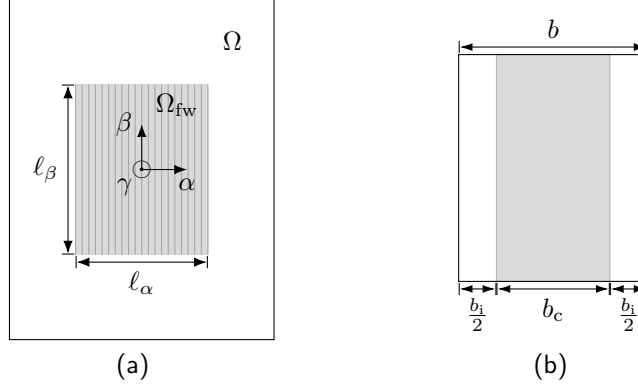


Figure 2: Geometry of a foil winding: (a) Cross-section of the foil winding domain Ω_{fw} inside the computational domain Ω with the local coordinate system (α, β, γ) . The unit vectors \vec{e}_α , \vec{e}_β and \vec{e}_γ point perpendicular to the foils, to the tips of the foils and in the direction of symmetry, respectively. (b) Cross-section of a single foil. The conducting material is in gray and the insulation material in white.

for all turns k , with \vec{J} being the current density. We assume that the foils are thin with respect to the skin depth, i.e., $b_c \ll \delta = \sqrt{\frac{2}{\omega\mu\sigma}}$, with the angular frequency ω , the permeability μ and the conductivity σ . With that, the current density can be assumed constant over the thickness of a foil. Since the conductivity in the insulation material σ_i is zero, the current density is only present in the conducting material. Consequently, (5) can be approximated using the conductivity of the conducting material σ_c with

$$i \approx b_c \int_{\Gamma(\alpha_k)} \vec{J} \cdot \vec{\zeta} \, dS = b_c \int_{\Gamma(\alpha_k)} \sigma_c \vec{E} \cdot \vec{\zeta} \, dS. \quad (6)$$

Herein, $\Gamma(\alpha)$ is the surface through the foil winding domain at position α , i.e.

$$\Gamma(\alpha) := \{\mathbf{f}(\alpha, \beta, \gamma) : \beta \in L_\beta, \gamma \in L_\gamma\} \subset \Omega_{\text{fw}}, \quad (7)$$

and α_k is the mid point coordinate of the k -th turn. Lastly, we insert the expression for \vec{E} and write

$$i \approx b \int_{\Gamma(\alpha_k)} \lambda \sigma_c \left(-\partial_t \vec{A} + \Phi \vec{\zeta} \right) \cdot \vec{\zeta} \, dS. \quad (8)$$

In the homogenized model, the single foils are not resolved anymore. The foil winding domain has constant anisotropic material parameters of a homogenized conductivity and reluctivity that are determined with a mixing rule [27].

Therefore, in the foil winding domain, we write

$$\sigma_\alpha = 0, \quad \sigma_\beta = \sigma_\gamma = \lambda\sigma_c + (1-\lambda)\sigma_i = \lambda\sigma_c, \quad (9a)$$

$$\nu_\alpha = \lambda\nu_c + (1-\lambda)\nu_i, \quad \nu_\beta = \nu_\gamma = \left(\frac{\lambda}{\nu_c} + \frac{(1-\lambda)}{\nu_i} \right)^{-1}. \quad (9b)$$

The current condition (8) has to hold for all α_k . For $N \rightarrow \infty$, we impose (8) for all $\alpha \in L_\alpha$. We end up with the final, homogenized system of equations

$$\operatorname{curl} \left(\nu \operatorname{curl} \vec{A} \right) + \sigma \partial_t \vec{A} - \sigma \Phi \vec{\zeta} = 0, \quad \text{in } \Omega \quad (10a)$$

$$\int_{\Gamma(\alpha)} \sigma \left(-\partial_t \vec{A} + \Phi \vec{\zeta} \right) \cdot \vec{\zeta} \, dS = \frac{i}{b}, \quad \text{in } L_\alpha \quad (10b)$$

with adequate initial values and boundary conditions on $\partial\Omega$. We choose, for simplicity of notation, a homogenous Dirichlet condition, i.e., $\vec{A} \times \vec{n} = 0$ on $\partial\Omega$ where \vec{n} is the outward pointing normal vector.

2.1 Discretized model

In the following, (10) is discretized using the Galerkin procedure [2, 22]. The vector potential \vec{A} is discretized with a finite set of standard FE edge functions $\vec{w}_j \in \mathbf{H}_0(\operatorname{curl}, \Omega)$. We assume that the distribution function $\vec{\zeta}$ can be expressed in terms of the same \vec{w}_j or is approximated by L2 projection. Finally, the voltage function Φ is discretized with another set of basis functions $\hat{p}_l \in H^1(L_\alpha)$ which are defined in the local coordinate system but can be transformed with

$$p_l(x, y, z) = \begin{cases} \hat{p}_l \circ f_\alpha^{-1}(x, y, z) & \text{if } (x, y, z) \in \Omega_{\text{fw}}, \\ 0 & \text{otherwise,} \end{cases} \quad (11)$$

where $f_\alpha^{-1}(x, y, z)$ denotes the α -component of the inverse of \mathbf{f} . This allows us to expand the fields in terms of the basis functions defined on Ω as

$$\vec{A} = \sum_{j=1}^{N_w} a_j \vec{w}_j, \quad \vec{\zeta} = \sum_{j=1}^{N_w} x_j \vec{w}_j \quad \text{and} \quad \Phi = \sum_{l=1}^{N_p} u_l p_l, \quad (12)$$

where we do not distinguish between the exact fields and their FE approximations.

Testing (10a) with edge functions \vec{w}_i and integration over the computational domain Ω yield the standard FE matrices $\mathbf{K}_\nu, \mathbf{M}_\sigma \in \mathbb{R}^{N_w \times N_w}$ and the vector $\mathbf{X}_\sigma \in \mathbb{R}^{N_w \times N_p}$. Their entries are

$$[\mathbf{K}_\nu]_{i,j} = \int_{\Omega} \nu \operatorname{curl} \vec{w}_j \cdot \operatorname{curl} \vec{w}_i \, dV, \quad (13)$$

$$[\mathbf{M}_\sigma]_{i,j} = \int_{\Omega} \sigma \vec{w}_j \cdot \vec{w}_i \, dV, \quad (14)$$

$$[\mathbf{X}_\sigma]_{i,l} = \int_{\Omega} \sigma p_l \vec{\zeta} \cdot \vec{w}_i \, dV. \quad (15)$$

Following the naming convention from mechanics, we call \mathbf{K}_σ the stiffness matrix and \mathbf{M}_σ the mass matrix. Since the distribution function ζ can be expressed in terms of the FE edge functions \vec{w}_j , see (12), it holds

$$[\mathbf{X}_\sigma]_{i,l} = \sum_j x_j \int_\Omega \sigma p_l \vec{w}_j \cdot \vec{w}_i \, dV \quad (16)$$

$$= [\mathbf{M}_{\sigma,l} \mathbf{x}]_i, \quad (17)$$

with the coefficients of the distribution function $[\mathbf{x}]_i = x_i$ and the (modified) mass matrix $[\mathbf{M}_{\sigma,l}]_{i,j} = \int_\Omega \sigma p_l \vec{w}_j \cdot \vec{w}_i \, dV$ containing the extra basis functions.

The current condition (10b) is tested with the basis functions p_k and integrated over the one-dimensional domain $\mathbf{f}(L_\alpha, \beta, \gamma)$ of homogenization, i.e.

$$\int_\Omega \sigma \left(-\partial_t \vec{A} + \Phi \vec{\zeta} \right) \cdot \vec{\zeta} p_k \, dV = \int_{\mathbf{f}(L_\alpha, \beta, \gamma)} \frac{i}{b} p_k \, ds. \quad (18)$$

This yields to the transpose of the already defined matrix \mathbf{X}_σ , the vector $\mathbf{c} \in \mathbb{R}^{N_p}$ and the turn-by-turn conductance matrix $\mathbf{G} \in \mathbb{R}^{N_p \times N_p}$, whose entries are defined as

$$[\mathbf{c}]_k = \frac{1}{b} \int_{\mathbf{f}(L_\alpha, \beta, \gamma)} p_k \, ds = \frac{N}{\ell_\alpha} \int_{\mathbf{f}(L_\alpha, \beta, \gamma)} p_k \, ds, \quad (19)$$

and

$$[\mathbf{G}]_{k,l} = \int_\Omega \sigma \vec{\zeta} \cdot \vec{\zeta} p_l p_k \, dV \quad (20)$$

$$= \sum_{i,j=1}^{N_w} x_i x_j \int_\Omega \sigma \vec{w}_i \cdot \vec{w}_j p_l p_k \, dV \quad (21)$$

$$= \mathbf{x}^\top \mathbf{M}_{\sigma,k,l} \mathbf{x}, \quad (22)$$

expressed in terms of the (modified) mass matrices $[\mathbf{M}_{\sigma,k,l}] = \int_\Omega \sigma \vec{w}_i \cdot \vec{w}_j p_l p_k \, dV$ involving both p_k and p_l .

The voltage drop v over the foil winding domain is the sum of the voltage drops over each foil, i.e.

$$v = \sum_{k=1}^N v_k. \quad (23)$$

With the voltage function, we can approximate the voltage drop over foil k as $v_k = \Phi(\mathbf{f}(\alpha_k, \cdot, \cdot))$. From there, it follows

$$v = \sum_k \Phi(\mathbf{f}(\alpha_k, \cdot, \cdot)) \approx \sum_k \frac{1}{\delta} \int_{\alpha_k - \frac{\delta}{2}}^{\alpha_k + \frac{\delta}{2}} \Phi(\mathbf{f}(\alpha, \cdot, \cdot)) \, d\alpha \quad (24)$$

$$= \frac{1}{\delta} \int_{L_\alpha} \Phi(\mathbf{f}(\alpha, \cdot, \cdot)) \, d\alpha \quad (25)$$

$$= \frac{1}{b} \int_{\mathbf{f}(L_\alpha, \beta, \gamma)} \Phi \, ds. \quad (26)$$

Consequently, the voltage can be expressed with $v = \mathbf{c}^\top \mathbf{u}$.

Finally, the discretized foil conductor model can be expressed in terms of the matrices above as

$$\mathbf{M}_\sigma \frac{d}{dt} \mathbf{a} + \mathbf{K}_\nu \mathbf{a} - \mathbf{X}_\sigma \mathbf{u} = \mathbf{0} \quad (27a)$$

$$-\mathbf{X}_\sigma^\top \frac{d}{dt} \mathbf{a} + \mathbf{G} \mathbf{u} - \mathbf{c} i = \mathbf{0} \quad (27b)$$

$$-\mathbf{c}^\top \mathbf{u} + v = 0 \quad (27c)$$

with appropriate initial values at some time t_0 . This three-dimensional model is a natural generalization to special cases found in literature, for example the two-dimensional model in Ref. [11], and it coincides with the model of Dular et al. in Ref. [14].

2.2 Alternative discretization of the turn-by-turn conductance matrix

We propose an alternative discretization of the turn-by-turn conductance matrix (20). We start by introducing the source electric field corresponding to voltage v_l as an explicit variable

$$\vec{E}_{s,l} = p_l \vec{\zeta} = \sum_{j=1}^{N_w} e_{l,j} \vec{w}_j \quad (28)$$

and use this in (20) such that

$$[\mathbf{G}_e]_{k,l} = \int_{\Omega} \sigma p_k \vec{\zeta} \cdot \vec{E}_{s,l} dV \quad (29)$$

$$= \sum_{i,j} x_i e_{l,j} \int_{\Omega} \sigma p_k \vec{w}_i \cdot \vec{w}_j dV \quad (30)$$

$$= \mathbf{x}^\top \mathbf{M}_{\sigma,k} \mathbf{e}_l \quad (31)$$

and for all $j = 1, \dots, N_w$

$$\int_{\Omega} \sigma \vec{w}_j \cdot \vec{E}_{s,l} dV = \int_{\Omega} \sigma \vec{w}_j \cdot (p_l \vec{\zeta}) dV \quad (32)$$

$$\sum_i e_{l,i} \int_{\Omega} \sigma \vec{w}_j \cdot \vec{w}_i dV = \sum_i x_i \int_{\Omega} \sigma p_l \vec{w}_j \cdot \vec{w}_i dV \quad (33)$$

$$\mathbf{M}_{\sigma} \mathbf{e}_l = \mathbf{M}_{\sigma,l} \mathbf{x}. \quad (34)$$

Plugging \mathbf{e}_l into the above equation yields another variant of the turn-by-turn conductance matrix, i.e.,

$$[\mathbf{G}_e]_{k,l} = \mathbf{x}^\top \mathbf{M}_{\sigma,k} \mathbf{M}_{\sigma}^+ \mathbf{M}_{\sigma,l} \mathbf{x}, \quad (35)$$

where \mathbf{M}_σ^+ denotes the (Moore-Penrose) pseudo-inverse of \mathbf{M}_σ . This mass matrix is singular because it only acts on degrees of freedom that are located in conductive domains. However, this is sufficient since the source electric fields are located exactly there.

Note that both definitions, i.e., (20) and (35), lead in general to different matrices for finitely many basis functions. However, both are consistent with the FE discretization and converge for $N_w, N_p \rightarrow \infty$ to the same solution.

2.3 Compatibility with solid conductor model

In Ref. [29], it is stated that the foil conductor model behaves as a solid conductor if a constant voltage function is chosen, i.e., $p_1 = 1$ is the only basis function ($N_p = 1$). In this special case the definitions (13) and (14) do not change but (17) naturally simplifies to

$$\mathbf{x}_{\text{sol}} = \mathbf{M}_\sigma \mathbf{x}. \quad (36)$$

Both the original (20) and the new discretization (35) of the turn-by-turn conductance matrix reduce to

$$G_{\text{sol}} = \mathbf{x}^\top \mathbf{M}_\sigma \mathbf{x} \quad (37)$$

$$= \mathbf{x}^\top \mathbf{M}_\sigma \mathbf{M}_\sigma^+ \mathbf{M}_\sigma \mathbf{x}. \quad (38)$$

From this, it follows that the foil conductor model is equivalent to the classic solid conductor model [26] for both variants of the conductance matrices. It reads

$$\mathbf{M}_\sigma \frac{d}{dt} \mathbf{a} + \mathbf{K}_\nu \mathbf{a} - \mathbf{x}_{\text{sol}} v = \mathbf{0} \quad (39a)$$

$$-\mathbf{x}_{\text{sol}}^\top \frac{d}{dt} \mathbf{a} + G_{\text{sol}} v - i = 0. \quad (39b)$$

since the third equation (27c) becomes trivial, i.e., $u_1 = v$, and can be plugged into the second (27b).

3 Circuit Compatibility

The conductor models, i.e., foil (27) and solid (39), provide the necessary coupling conditions for circuits, i.e., they allow to excite the electromagnetic fields in terms of currents and voltages. Since the mid 70s, the most common formalism implemented in circuit simulators is the modified nodal analysis (MNA) [19]. Its main advantages are sparse system matrices that are easy to assemble and its robustness with respect to topological changes, e.g., switching. While the MNA is formulated in less unknowns than for example sparse tableau analysis [17], it does not aim for a minimal set of degrees of freedom. One consequence of this redundancy is that the resulting system consists of differential and algebraic equations (DAEs) rather than ordinary differential equations (ODEs).

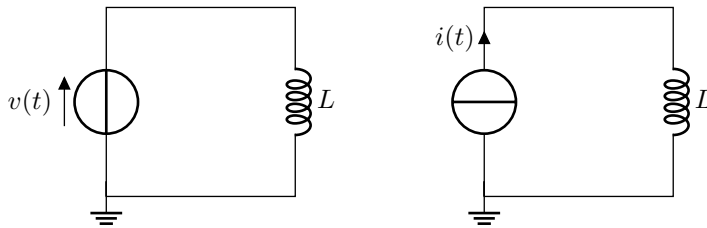


Figure 3: Voltage- (left) and current-driven (right) inductor.

Common issues related to the numerical treatment of DAEs are the difficulty of finding consistent initial conditions and the sensitivity towards perturbations [18].

3.1 Sensitivity with respect to perturbations

To illustrate these numerical difficulties, we consider a simple inductor model in flux-oriented form, i.e.,

$$\frac{d}{dt}\psi(t) = v(t) \quad (40a)$$

$$\psi(t) = Li(t) \quad (40b)$$

for $t \in (t_0, t_{\text{end}}]$. The equations describe a relation between currents and voltages. Let us investigate the voltage- and current-driven-case separately, see Fig. 3.

3.1.1 Voltage-driven case

For a given voltage v the problem is described in terms of a differential equation defining the flux ψ and an algebraic equation for the current i . After time-differentiation of (40b) one obtains a purely differential problem. The solution is

$$i(t) = \frac{1}{L} \left(\psi_0 + \int_{t_0}^t v(s) ds \right) \quad (41)$$

with an arbitrary flux $\psi(t_0) = \psi_0$ as initial condition.

3.1.2 Current-driven case

If the current i is given, then ψ is fixed by an algebraic relation and the solution is

$$v(t) = L \frac{d}{dt} i(t). \quad (42)$$

This is an algebraic equation that does not allow to freely specify an initial condition or more precisely: only $v(t_0) = v_0 := L \frac{d}{dt} i(t)|_{t_0}$ is consistent. Note

that this equation is obtained with one time-differentiation of (40b). Only after a second differentiation an explicit ODE for $\frac{d}{dt}v$ can be obtained.

3.2 Differential index

The sensitivity of the solution with respect to perturbations is very different in the systems of Section 3.1.1 and 3.1.2. Let us consider the following particular current excitation for the current-driven case

$$i(t) = I_1 \sin(2\pi f_1 t) + I_2 \sin(2\pi f_2 t) \quad (43)$$

where the second amplitude shall be almost negligible $I_2 \ll I_1$ but at very high frequency $f_2 \gg I_1/I_2 f_1$. Due to the time-derivative in (42) the solution in the current-driven case will be seriously perturbed, i.e., the second term with amplitude $2\pi f_2 I_2$ becomes dominant. On the other hand, a similarly perturbed voltage source would not significantly affect the current of the voltage-driven case (41) since there, in the solution, the sum of the sine waves appears integrated in time instead of differentiated.

This motivates the introduction of the number of time-differentiations as a measure of sensitivity and classification of DAEs. In this context, the notion of index of a DAE is proposed. Several definitions exist. We use the following:

Definition 1. (*Differential index* [7]) *A solvable and sufficiently smooth system of DAEs $\mathbf{f}(\mathbf{x}', \mathbf{x}, t) = \mathbf{0}$ is said to have differential index m , if m is the minimum number of differentiations*

$$\mathbf{f}(\mathbf{x}', \mathbf{x}, t) = \mathbf{0}, \quad \frac{d}{dt}\mathbf{f}(\mathbf{x}', \mathbf{x}, t) = \mathbf{0}, \quad \dots, \quad \frac{d^m}{dt^m}\mathbf{f}(\mathbf{x}', \mathbf{x}, t) = \mathbf{0},$$

that allow the extraction of an explicit ordinary differential system with only algebraic manipulations.

For circuits modeled with MNA containing classical lumped circuit elements, the differential index is known and depends on the topology of the circuit [16]. The index is 2 at maximum. The following theorem states the condition for this case, however, without formulating all necessary assumptions for which the reader is referred to the original paper.

Theorem 1. (*Differential index of circuits* [16]) *Circuits modeled with MNA lead to systems of DAEs with differential index 2 if, and only if, at least one of the following conditions is fulfilled. The circuit contains*

- (i) *cutsets of branches which contain only inductors and current sources ("LI-cutsets").*
- (ii) *loops of branches which contain only capacitors and voltage sources ("CV-loops") with at least one voltage source.*

Otherwise, the circuit has differential index 1.

The theorem is immediately applicable to our two simple inductor examples. The first case, Section 3.1.1, is a series connection of an inductor and a voltage source which is at most index 1 and harmless. The second example, Section 3.1.2, forms a LI -cutset and may lead to numerical problems, e.g., high sensitivity towards noise as observed.

3.3 Classifications

Generalized circuit elements have been introduced in Ref. [10] to classify field models as refined elements and to include them in the index result of Theorem 1. Resistance-like, inductance-like and capacitance-like elements are defined. Classical resistances, capacitors and inductors, as well as charge formulated capacitances and flux formulated inductances have been shown to correspond to their generalized circuit elements. The type of generalized element, that the field model is, gives an intuition how the model will behave in an external circuit. Given the intuitively inductive nature of the foil conductor model, we focus on the introduction of the inductance-like element. The resistance-like element is briefly remarked.

In the following, a simplified version of the (strongly) inductance-like element definition [10] will be used. The definition is more restrictive but still sufficient for the analysis of linear systems such as the foil conductor model discussed here.

Definition 2. (*Inductance-like element*) *A circuit element is called inductance-like, if with only one time differentiation its constitutive equations can be transformed into the form*

$$\frac{d}{dt}\mathbf{x} = \mathbf{f}_{\mathbf{x}}(\mathbf{x}, i, v, t) \quad (44a)$$

$$\frac{d}{dt}i = g_L(\mathbf{x}, i, v, t) \quad (44b)$$

where \mathbf{x} are ‘internal’ variables that are not explicitly coupled to the circuit (e.g., vector potentials). Additionally,

$$\partial_v g_L(\mathbf{x}, i, v, t) := L \quad (45)$$

is required to be positive (definite).

In addition to inductance-like, Ref. [10] defines resistance-like and capacitance-like elements. Roughly speaking, a (simplified) resistance-like element is defined similarly to the inductance-like element in Definition 2, with the key difference being that the implicit relation between the current i and the voltage v is

$$\frac{d}{dt}i = g_R\left(\frac{d}{dt}v, \mathbf{x}, i, v, t\right), \quad (46)$$

where $\partial_{v'} g_R(v', \mathbf{x}, i, v, t) := G_R$ is positive (definite). For a formal definition of resistance-like as well as capacitance-like elements we refer to Ref. [10].

The conclusions drawn in Section 3.2 for the differential index of the circuits containing only an inductance and a source as well as Theorem 1 remain unchanged if the elements are replaced with their generalized definitions.

3.4 Inductance-like behavior

In this section, the previously introduced mathematical concepts are utilized to analyze the foil conductor model which uses the proposed turn-by-turn conductance matrix (35). We seek to prove that the model is an inductance-like element.

Assumption 1. *Gauged field formulation with consistent excitation*

- (i) \mathbf{X}_σ has full column rank.
- (ii) The field formulation is adequately gauged such that the matrix pencil $\tau\mathbf{M}_\sigma + \mathbf{K}_\nu$ is regular, i.e., $\det(\tau\mathbf{M}_\sigma + \mathbf{K}_\nu) \neq 0$ for a $\tau \in \mathbb{R}$.

Property (i) describes a consistent excitation. The condition for (ii) is automatically fulfilled when the calculation is done in 2D. In 3D, an additional gauging condition needs to be imposed, such as, e.g., a tree-cotree gauge [1].

Using Property (i) of Assumption 1 leads to \mathbf{G}_e being invertible. Consequently, the system of equations (27) can be written as

$$\underbrace{(\mathbf{M}_\sigma - \mathbf{X}_\sigma \mathbf{G}_e^{-1} \mathbf{X}_\sigma^\top)}_{:=\bar{\mathbf{M}}} \frac{d}{dt} \mathbf{a} + \mathbf{K}_\nu \mathbf{a} = \underbrace{\mathbf{X}_\sigma \mathbf{G}_e^{-1} \mathbf{c}}_{:=\bar{\mathbf{x}}} i \quad (47a)$$

$$\underbrace{\mathbf{c}^\top \mathbf{G}_e^{-1} \mathbf{X}_\sigma^\top}_{:=\bar{\mathbf{x}}^\top} \frac{d}{dt} \mathbf{a} + \underbrace{\mathbf{c}^\top \mathbf{G}_e^{-1} \mathbf{c}}_{:=R} i = v \quad (47b)$$

by solving (27b) with respect to \mathbf{u} , and substituting it in (27a) and (27c). Note that (47) has the same structure as the stranded conductor model, which is known to be an inductance-like element [9].

Proposition 1. *The foil conductor model according to (47) using the proposed turn-by-turn conductance matrix (35) is an inductance-like element.*

Proof. The proof is presented in Appendix A. □

Note that \mathbf{u} is part of the internal variables of the inductance-like element in the foil conductor model and is not explicitly coupled to the circuit. Therefore, its behavior will not influence the circuit itself, and it can be left out of the proof. Examinations suggest that it is an index-2 variable. This, however, does not influence the index of the circuit's variables.

3.5 (Singularly perturbed) Resistance-like behavior

Similarly to the analysis for (47), the original system (27) with the original turn-by-turn conductance matrix \mathbf{G} as defined in (20) can be classified according to the generalized circuit elements of Ref. [10].

Proposition 2. *The foil conductor model (27) with the original turn-by-turn conductance matrix (20) is a resistance-like element.*

Proof. The proof is given in Appendix B. □

The key difference between both cases is that, whereas in our redefined conductance we replace \mathbf{G} with \mathbf{G}_e and, therefore, $\frac{\partial g_R}{\partial v'} = (\mathbf{c}^\top (\mathbf{G} - \mathbf{G}_e)^{-1} \mathbf{c})^{-1} = 0$ (see Appendix B), in the original conductance computation, $\mathbf{G} \neq \mathbf{G}_e$. Intuitively, this inconsistency arises as \mathbf{G} corresponds to the natural discretization of the foil conductor's conductance but only \mathbf{G}_e is consistent with the discrete spaces spanned by the finite element matrices.

Remark. We say the foil conductor model (27) with the original turn-by-turn conductance matrix (20) is singularly perturbed resistance-like, as its resistance-like behavior depends on the positive definiteness of $\frac{\partial g_R}{\partial v'} = (\mathbf{c}^\top (\mathbf{G} - \mathbf{G}_e)^{-1} \mathbf{c})^{-1}$. This expression imposes the (linear) relation between $\frac{d}{dt}i$ and $\frac{d}{dt}v$ in (46). Thus, if the term is positive definite, the element is resistance-like. However, when refining the finite element discretization ($N_w, N_p \rightarrow \infty$), that term tends to zero, and the model degenerates into an inductance-like element.

4 Numerical Results

A numerical implementation of the foil conductor model according to (27) is done for both of the turn-by-turn conductance matrix definitions (20) and (35) using the FE simulation framework *Pyrit* [8]. The considered 2D axisymmetric modeling domain is shown in Fig. 4. Table 1 contains the simulation specifications and the values used for the material parameters. Discretization in the time domain is done using the implicit Euler method with a constant time-step length.

The first test case is to demonstrate the consequences of Proposition 1 for the simulation of the foil conductor model. The proposed new turn-by-turn conductance matrix (35) is used, and the modeling domain is spatially discretized with a coarse mesh consisting of 1397 nodes. A voltage-driven foil winding is known to yield a system of DAEs with differentiation index 1, whereas the current-driven counterpart is an index-2 system. The sensitivity towards noise that these systems exhibit is examined by exciting them with a sinusoidal input which is perturbed with an additional sinusoid with small amplitude but high frequency. The magnitude of both the source voltage and current is given as $\sin(2\pi ft) + \epsilon \sin(2\pi f_\epsilon t)$.

Figure 5a shows the voltage over the current-fed foil winding. The perturbations of the source current are clearly amplified in the voltage output over

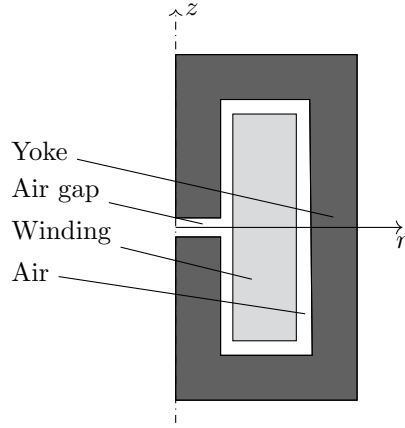


Figure 4: Simulation domain for the numerical tests.

Table 1: Simulation specifications and material parameters.

Quantity	Symbol	Value
Number of voltage basis functions	N_p	5
Number of foils	N	50
Fill factor	λ	0.8
Foil thickness	b	0.28 mm
Foil height	ℓ_β	50 mm
Air gap length	-	4.2 mm
Yoke height	-	76.2 mm
Yoke outer radius	-	40 mm
Frequency	f	50 Hz
Perturbation frequency	f_ϵ	$2\pi \cdot 10^{10}$ Hz
Perturbation amplitude	ϵ	10^{-3}
Foil winding conductivity	σ	$6 \cdot 10^7 \text{ S m}^{-1}$
Yoke conductivity	-	10 S m^{-1}
Yoke relative permeability	-	1000

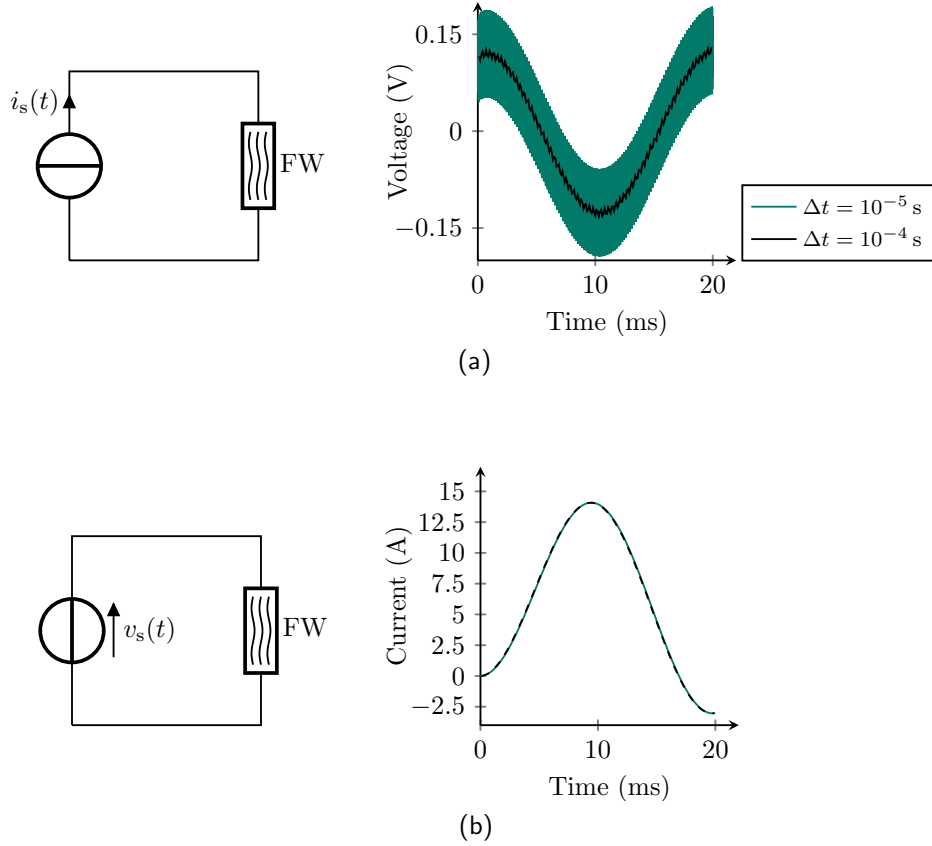


Figure 5: Current- and voltage-driven foil winding. (a) The perturbations that are added to the source current are amplified in the voltage over the foil winding. (b) No amplification of the perturbations of the source voltage occurs.

the foil winding, and the amplification increases when the time-step length is reduced. When the model is excited with a voltage source, no perturbations are visible in the current through the foil winding, as can be seen in Fig. 5b. This corresponds to the expected behavior of an inductance-like element, which is less sensitive towards perturbations when excited with a voltage source than with a current source.

In the following, we compare the numerical behavior of the foil conductor model when using the two different turn-by-turn conductance matrices. The mismatch between the matrices $\|\mathbf{G} - \mathbf{G}_e\|$ is varied by refining the mesh. The earlier simulation setting is kept, and now only the current-driven model is examined. A time-step length of $\Delta t = 10^{-4}$ s is used.

Figure 6 shows the effect of reducing $\|\mathbf{G} - \mathbf{G}_e\|$ on the simulated voltage waveform. When $\|\mathbf{G} - \mathbf{G}_e\| \rightarrow 0$ through mesh refinement, the models coincide (numerically). This shows how the foil conductor model with the turn-by-turn

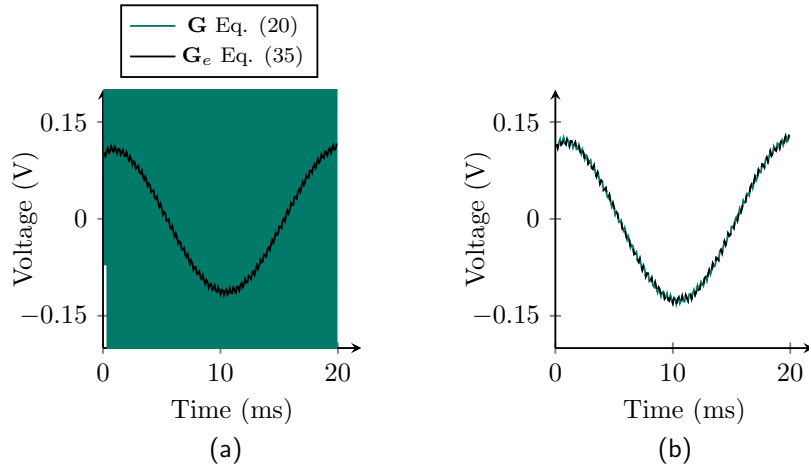


Figure 6: The voltage over the current driven foil winding with the different turn-by-turn conductance matrix definitions and mesh refinement. Different meshes with (a) 103 and (b) 1397 nodes.

conductance matrix \mathbf{G} degenerates into an inductance-like element. With increasing $\|\mathbf{G} - \mathbf{G}_e\|$, the model becomes increasingly unstable and eventually diverges. A similar instability is not observed when using the proposed matrix \mathbf{G}_e .

5 Conclusion

This paper demonstrates that the classical definition of the foil conductor model is inconsistent in terms of circuit theory, i.e., the field model behaves in a circuit rather like a (singularly perturbed) resistor instead of an inductor. For coarse discretizations this may lead to instabilities in the time-stepping process. It is shown that a simple modification of the turn-by-turn conductance matrix mitigates this problem and leads provably to an inductance-like behavior. This is consistent with the behavior of eddy current fields excited with other conductor models such as the solid and stranded conductor ones. The modification is always consistent, easy to implement in existing codes, and only marginally increases the computational cost.

Appendix A Proof of Proposition 1

Define projector $\bar{\mathbf{Q}}$ onto $\ker(\bar{\mathbf{M}})$, and its complementary $\bar{\mathbf{P}} = \mathbf{I} - \bar{\mathbf{Q}}$. The projectors enable splitting (47a)

$$\bar{\mathbf{Q}}^\top \mathbf{K}_\nu \mathbf{a} = \bar{\mathbf{Q}}^\top \bar{\mathbf{x}} i \quad (48a)$$

$$\bar{\mathbf{M}} \frac{d}{dt} \mathbf{a} + \bar{\mathbf{P}}^\top \mathbf{K}_\nu \mathbf{a} = \bar{\mathbf{P}}^\top \bar{\mathbf{x}} i. \quad (48b)$$

The matrix $\bar{\mathbf{M}} + \bar{\mathbf{Q}}^\top \bar{\mathbf{Q}}$ is symmetric positive definite due to the definition of projector matrices and the symmetry of $\bar{\mathbf{M}}$. Multiplication of (48b) with $(\bar{\mathbf{M}} + \bar{\mathbf{Q}}^\top \bar{\mathbf{Q}})^{-1}$ and carrying out only algebraic manipulations yields

$$\begin{aligned} \bar{\mathbf{P}} \frac{d}{dt} \mathbf{a} &= (\bar{\mathbf{M}} + \bar{\mathbf{Q}}^\top \bar{\mathbf{Q}})^{-1} (-\bar{\mathbf{P}}^\top \mathbf{K}_\nu \mathbf{a} + \bar{\mathbf{P}}^\top \bar{\mathbf{x}} i) \\ &= \mathbf{f}_\mathbf{P}(\mathbf{a}, i). \end{aligned} \quad (49)$$

One differentiation of (48a) with respect to time, and multiplication by $(\bar{\mathbf{Q}}^\top \mathbf{K}_\nu \bar{\mathbf{Q}} + \bar{\mathbf{P}}^\top \bar{\mathbf{P}})^{-1}$ gives

$$\bar{\mathbf{Q}} \frac{d}{dt} \mathbf{a} = (\bar{\mathbf{Q}}^\top \mathbf{K}_\nu \bar{\mathbf{Q}} + \bar{\mathbf{P}}^\top \bar{\mathbf{P}})^{-1} \left(-\bar{\mathbf{Q}}^\top \mathbf{K}_\nu \bar{\mathbf{P}} \frac{d}{dt} \mathbf{a} + \bar{\mathbf{Q}}^\top \bar{\mathbf{x}} \frac{d}{dt} i \right). \quad (50)$$

Property (ii) of Assumption 1 ensures that the matrix $\bar{\mathbf{Q}}^\top \mathbf{K}_\nu \bar{\mathbf{Q}} + \bar{\mathbf{P}}^\top \bar{\mathbf{P}}$ is positive definite. Substituting $\frac{d}{dt} \mathbf{a}$ in (47b) allows solving the resulting equation with respect to the time derivative of the current

$$\begin{aligned} \frac{d}{dt} i &= L^{-1} \left[v - Ri - \bar{\mathbf{x}}^\top \left(\mathbf{I} - \bar{\mathbf{Q}} (\bar{\mathbf{Q}}^\top \mathbf{K}_\nu \bar{\mathbf{Q}} + \bar{\mathbf{P}}^\top \bar{\mathbf{P}})^{-1} \bar{\mathbf{Q}}^\top \mathbf{K}_\nu \right) \mathbf{f}_\mathbf{P}(\mathbf{a}, i) \right] \\ &= f_i(\mathbf{a}, i, v), \end{aligned} \quad (51)$$

where \mathbf{I} is an identity matrix. The previous step required the inversion of $L = \bar{\mathbf{x}}^\top \bar{\mathbf{Q}} (\bar{\mathbf{Q}}^\top \mathbf{K}_\nu \bar{\mathbf{Q}} + \bar{\mathbf{P}}^\top \bar{\mathbf{P}})^{-1} \bar{\mathbf{Q}}^\top \bar{\mathbf{x}}$, which is always possible when $L \neq 0$. This is guaranteed as it can be shown that $\bar{\mathbf{Q}}^\top \bar{\mathbf{x}}$ has full column rank. Consequently, L is positive (definite).

Substituting $\frac{d}{dt} i$ to (50) yields $\bar{\mathbf{Q}} \frac{d}{dt} \mathbf{a} = \mathbf{f}_\mathbf{Q}(\mathbf{a}, i, v)$. The explicit ODEs in Definition 2 have been obtained with only one time differentiation of (47), where the internal variables $\mathbf{x} = \mathbf{a}$.

Appendix B Proof of Proposition 2

Similarly as in the proof in Appendix A, we start by splitting (this time) the original discretization of the eddy current equation (27a) with the projectors \mathbf{Q}_σ onto $\ker \mathbf{M}_\sigma$ and its complementary \mathbf{P}_σ . This leads to

$$\mathbf{M}_\sigma \frac{d}{dt} \mathbf{a} + \mathbf{P}_\sigma \mathbf{K}_\nu \mathbf{a} - \mathbf{P}_\sigma \mathbf{X}_\sigma \mathbf{u} = \mathbf{0} \quad (52a)$$

$$\mathbf{Q}_\sigma \mathbf{K}_\nu \mathbf{a} - \mathbf{Q}_\sigma \mathbf{X}_\sigma \mathbf{u} = \mathbf{0}. \quad (52b)$$

With (52a) one obtains

$$\mathbf{P}_\sigma \frac{d}{dt} \mathbf{a} = (\mathbf{M}_\sigma + \mathbf{Q}_\sigma^\top \mathbf{Q}_\sigma)^{-1} (-\mathbf{P}_\sigma \mathbf{K}_\nu \mathbf{a} + \mathbf{P}_\sigma \mathbf{X}_\sigma \mathbf{u}). \quad (53)$$

One time differentiation of (52b) and using the property that $\mathbf{Q}_\sigma \mathbf{X}_\sigma = 0$ due to \mathbf{X}_σ being zero outside the conducting region, we have

$$\begin{aligned} \mathbf{Q}_\sigma \frac{d}{dt} \mathbf{a} = & -(\mathbf{Q}_\sigma \mathbf{K}_\nu \mathbf{Q}_\sigma + \mathbf{P}_\sigma^\top \mathbf{P}_\sigma)^{-1} \mathbf{Q}_\sigma \mathbf{K}_\nu \\ & (\mathbf{M}_\sigma + \mathbf{Q}_\sigma^\top \mathbf{Q}_\sigma)^{-1} \mathbf{P}_\sigma (\mathbf{K}_\nu \mathbf{a} - \mathbf{X}_\sigma \mathbf{u}). \end{aligned} \quad (54)$$

With these two equations we obtained an ODE for $\frac{d}{dt} \mathbf{a} = \mathbf{P}_\sigma \frac{d}{dt} \mathbf{a} + \mathbf{Q}_\sigma \frac{d}{dt} \mathbf{a}$ with at most one time differentiation of the original system. Inserting now (53) into the equation for \mathbf{u} , (27b) leads to

$$\begin{aligned} \mathbf{u} = & \left(\mathbf{G} - \mathbf{X}_\sigma^\top (\mathbf{M}_\sigma + \mathbf{Q}_\sigma^\top \mathbf{Q}_\sigma)^{-1} \mathbf{X}_\sigma \right)^{-1} \\ & \left(-\mathbf{X}_\sigma^\top (\mathbf{M}_\sigma + \mathbf{Q}_\sigma^\top \mathbf{Q}_\sigma)^{-1} \mathbf{P}_\sigma \mathbf{K}_\nu \mathbf{a} + \mathbf{c} i \right). \end{aligned} \quad (55)$$

Differentiating the latter expression once in time and using (53)-(54) gives

$$\frac{d}{dt} \mathbf{u} = (\mathbf{G} - \mathbf{X}_\sigma^\top (\mathbf{M}_\sigma + \mathbf{Q}_\sigma^\top \mathbf{Q}_\sigma)^{-1} \mathbf{X}_\sigma)^{-1} \mathbf{c} \frac{d}{dt} i + \mathbf{f}_u(\mathbf{a}, \mathbf{u}), \quad (56)$$

which is an ODE-like expression for $\frac{d}{dt} \mathbf{u}$. Note that, in contrast to the formal definition of a resistance-like element, $\frac{d}{dt} \mathbf{u}$ depends on $\frac{d}{dt} i$. This, however, does not change the index results of Ref. [10] and therefore the element still has the same behavior as a resistance-like element within a circuit. Now that we have obtained expressions for the internal variables of the element $\frac{d}{dt} \mathbf{a}$ and $\frac{d}{dt} \mathbf{u}$, we look for the final relation between the current i and voltage v . This is recovered by differentiating (27c) once and inserting (56). Hereby, the voltage-to-current relation

$$\frac{d}{dt} v = \mathbf{c}^\top (\mathbf{G} - \mathbf{X}_\sigma^\top \mathbf{M}_\sigma^+ \mathbf{X}_\sigma)^{-1} \mathbf{c} \frac{d}{dt} i + \mathbf{c}^\top \mathbf{f}_u(\mathbf{a}, \mathbf{u}), \quad (57)$$

which corresponds to a strongly resistance-like element if

$$\frac{\partial g_R}{\partial v'} = (\mathbf{c}^\top (\mathbf{G} - \mathbf{X}_\sigma^\top \mathbf{M}_\sigma^+ \mathbf{X}_\sigma)^{-1} \mathbf{c})^{-1}$$

is positive definite. This is the case as long as $\mathbf{G} - \mathbf{X}_\sigma^\top \mathbf{M}_\sigma^+ \mathbf{X}_\sigma$ is nonsingular. In the last expressions we have replaced $\mathbf{X}_\sigma^\top (\mathbf{M}_\sigma + \mathbf{Q}_\sigma^\top \mathbf{Q}_\sigma)^{-1} \mathbf{X}_\sigma$ by $\mathbf{X}_\sigma^\top \mathbf{M}_\sigma^+ \mathbf{X}_\sigma$ with the Moore-Penrose pseudoinverse \mathbf{M}_σ^+ . This is done to illustrate why $\mathbf{G}_e = \mathbf{X}_\sigma^\top \mathbf{M}_\sigma^+ \mathbf{X}_\sigma$ has been chosen and is possible because $\mathbf{Q}_\sigma \mathbf{X}_\sigma = 0$ due to construction and therefore both expressions are equivalent.

Acknowledgments

The work of Elias Paakkunainen and Jonas Bundschuh is supported by the Graduate School CE within the Centre for Computational Engineering at Technische Universität Darmstadt. Additionally, support from the German Science Foundation (DFG project 436819664) is acknowledged.

References

- [1] R. Albanese and G. Rubinacci, Integral formulation for 3d eddy-current computation using edge elements, *IEE Proc. Sci. Meas. Tech.* **135** (1988) 457–462.
- [2] A. Alonso Rodríguez and A. Valli, *Eddy Current Approximation of Maxwell Equations*, volume 4 of *Modeling, Simulation and Applications* (Springer, 2010).
- [3] A. Bartel, S. Baumanns and S. Schöps, Structural analysis of electrical circuits including magnetoquasistatic devices, *APNUM* **61** (2011) 1257–1270.
- [4] A. Bartel and M. Günther, PDAEs in refined electric network modeling, *SIAM Rev.* **60** (2018) 56–91.
- [5] G. Bedrosian, A new method for coupling finite element field solutions with external circuits and kinematics, *IEEE Trans. Magn.* **29** (1993) 1664–1668.
- [6] G. Benderskaya, M. Clemens, H. De Gersem and T. Weiland, Embedded Runge-Kutta methods for field-circuit coupled problems with switching elements, *IEEE Trans. Magn.* **41** (2005) 1612–1615.
- [7] K. E. Brenan, S. L. Campbell and L. R. Petzold, *Numerical Solution of Initial-Value Problems in Differential-Algebraic Equations* (Society for Industrial and Applied Mathematics, 1995).
- [8] J. Bundschuh, M. G. Ruppert and Y. Späck-Leigsnering, Pyrit: A finite element based field simulation software written in Python, Preprint arxiv:2210.11983, Cornell University, 2022.
- [9] I. Cortes Garcia, H. De Gersem and S. Schöps, A structural analysis of field/circuit coupled problems based on a generalised circuit element, *Numer. Algorithm.* **83** (2020) 373–394.
- [10] I. Cortes Garcia, S. Schöps, C. Strohm and C. Tischendorf, Generalized elements for a structural analysis of circuits, in *Progress in Differential-Algebraic Equations II* (Springer, 2020), Differential-Algebraic Equations Forum.

- [11] H. De Gersem and K. Hameyer, A finite element model for foil winding simulation, *IEEE Trans. Magn.* **37** (2001) 3472–3432.
- [12] H. De Gersem, R. Mertens, D. Lahaye, S. Vandewalle and K. Hameyer, Solution strategies for transient, field-circuit coupled systems, *IEEE Trans. Magn.* **36** (2000) 1531–1534.
- [13] P. Dular, Dual magnetodynamic finite element formulations with natural definitions of global quantities for electric circuit coupling, in *Scientific Computing in Electrical Engineering — Proceedings of the 3rd International Workshop, August 20-23, 2000, Warnemünde, Germany* (Springer, 2001), pp. 367–378.
- [14] P. Dular and C. Geuzaine, Spatially dependent global quantities associated with 2-d and 3-d magnetic vector potential formulations for foil winding modeling, *IEEE Trans. Magn.* **38** (2002) 633–636.
- [15] R. Escarela-Perez, E. Melgoza and J. Alvarez-Ramirez, Systematic coupling of multiple magnetic field systems and circuits using finite element and modified nodal analyses, *IEEE Trans. Magn.* **47** (2011) 207–213.
- [16] D. Estévez Schwarz and C. Tischendorf, Structural analysis of electric circuits and consequences for MNA, *Int. J. Circ. Theor. Appl.* **28** (2000) 131–162.
- [17] G. Hachtel, R. Brayton and F. Gustavson, The sparse tableau approach to network analysis and design, *IEEE Trans. Circ. Theor.* **18** (1971) 101–113.
- [18] E. Hairer, S. P. Nørsett and G. Wanner, *Solving Ordinary Differential Equations II: Stiff and Differential-Algebraic Problems*, Springer Series in Computational Mathematics (Springer, 2002), 2 edition.
- [19] C.-W. Ho, A. E. Ruehli and P. A. Brennan, The modified nodal approach to network analysis, *IEEE Trans. Circ. Syst.* **22** (1975) 504–509.
- [20] S. Kanerva, Data transfer methodology between a FEM program and a system simulator, in *Proceedings of the Fifth International Conference on Electrical Machines and Systems, 2001. ICEMS 2001* (2001), volume 2, pp. 1121–1124.
- [21] M. Maciejewski, I. Cortes Garcia, S. Schöps, B. Auchmann, L. Bortot, M. Prioli and A. Verweij, Application of the waveform relaxation technique to the co-simulation of power converter controller and electrical circuit models, in *22nd International Conference on Methods and Models in Automation and Robotics (MMAR 2017)* (IEEE, 2017), pp. 837–842.
- [22] P. Monk, *Finite Element Methods for Maxwell's Equations* (Oxford University Press, 2003).

- [23] S. J. Salon, M. J. DeBortoli and R. Palma Zambrano, Coupling of transient fields, circuits, and motion using finite element analysis, *J. Electromagn. Waves Appl.* **4** (1990) 1077–1106.
- [24] S. Schöps, A. Bartel, H. De Gersem and M. Günther, DAE-index and convergence analysis of lumped electric circuits refined by 3-d MQS conductor models, in *Scientific Computing in Electrical Engineering SCEE 2008* (Springer, 2010), volume 14 of *Mathematics in Industry*, pp. 341–350.
- [25] S. Schöps, H. De Gersem and A. Bartel, A cosimulation framework for multirate time-integration of field/circuit coupled problems, *IEEE Trans. Magn.* **46** (2010) 3233–3236.
- [26] S. Schöps, H. De Gersem and T. Weiland, Winding functions in transient magnetoquasistatic field-circuit coupled simulations, *COMPEL* **32** (2013) 2063–2083.
- [27] A. Sihvola, *Electromagnetic Mixing Formulas and Applications* (IET, 1999).
- [28] I. A. Tsukerman, Finite element differential-algebraic systems for eddy current problems, *Numer. Algorithm.* **31** (2002) 319–335.
- [29] C. A. Valdivieso, G. Meunier, B. Ramdane, J. Gyselinck, C. Guerin and R. V. Sabariego, Time-domain homogenization of foil windings in 2-D axisymmetric finite-element models, *IEEE Trans. Power Deliv.* **36** (2021) 1264–1269.